Songklanakarin J. Sci. Technol.
41 (5), 966-973, Sep. - Oct. 2019

http://www.sjst.psu.ac.th

Original Article

The effect of hemispherical dimple spacing on flow structure and heat transfer characteristics of internal flow using CFD

Ye Min Oo[1], Makatar Wae-hayee[1*], Kamil Abdullah[2], and Chayut Nuntadusit[1]

[1]*Energy Technology Research Center, Department of Mechanical Engineering, Faculty of Engineering, Prince of Songkla University, Hat Yai, Songkhla, 90112 Thailand*

[2]*Department of Energy and Thermofluid Engineering, Faculty of Mechanical and Manufacturing Engineering, Universiti Tun Hussein Onn Malaysia, Johor, 86400 Malaysia*

Received: 30 October 2017; Revised: 3 April 2018; Accepted: 23 May 2018

Abstract

A simulation study of flow and heat transfer on a dimpled surface is presented. A 3-D model was tested in a wind tunnel with rectangular cross section. A row of dimples with inline arrangement were formed on the internal wind tunnel surface, so that the centerline of dimples was perpendicular to the air flow. The dimples were made with 40 mm diameter sphere, and the printed diameter of dimples on the surface was D=26.4 mm. The depth of a dimple was H=0.2D. The dimple-to-dimple spacings tested were S=1.125D, 1.25D, 1.5D and 2D. The Reynolds number of internal flow, based on the hydraulic diameter of the wind tunnel, was 20,000. The fluid flow and heat transfer were numerically solved using a Shear Stress Transport (SST) k-ω turbulence model. The results show that at S=1.125D, peak Nusselt numbers downstream of the dimples were found in two regions, whereas for cases with S≥1.25D there was a single such region.

Keywords: CFD, dimple, heat transfer, turbine blade cooling

1. Introduction

Various techniques are used to improve heat transfer for the cooling of gas turbine engine passages and turbine airfoils. Heat transfer at a fluid solid interface is the main barrier to improve in various engineering applications, such as automotive and aerospace components, heating and refrigerating, solar collectors, and electronic devices as described in Heo, Seo, Ku, and Kang (2011), Lan, Xie, and Zhang (2011). For the past decades, tremendous efforts have been made to improve efficiency and performance of thermal equipment, enabling reducing their size, weight and cost. Generally, convective heat transfer can be improved by active and/or passive techniques. Among the well-known passive techniques to enhance heat transfer are swirl flow devices Ligrani, Oliveira, and Blaskovich (2003), surface tension devices, rough surfaces Kurniawan, Kiswanto, and Ko (2017), Ligrani *et al*. (2011), pin fins (Ligrani *et al*., 2011), ribbed turbulators (Ligrani *et al*., 2011) and surfaces with dimples Rao, Li, and Feng (2015), Vorayos, Katkhaw, Kiatsiriroat, and Nuntaphan (2016), Xie, Qu, and Zhang (2015). Dimplesare regarded as most effective structures to enhance heat transfer rates without significant pressure drop or flow resistance.

Mahmood *et al*. (2000) conducted a wind tunnel investigation on an array of hemispherical dimples with staggered arrangement. They reported the formation of large vortex pairs ejected from the dimple cavities. Other studies on flow structures involving dimples have been reported by Ligrani, Harrison, Mahmmod, and Hill (2001), Shin, Lee, Park, and Kwak (2009), Won and Ligrani (2007), and Won, Zhang, and Ligrani (2005).

Recent studies on flow structures involving dimples have been carried out by numerical CFD simulations. Low cost and rapid experiments are two preferred aspects of the CFD approach. Another advantage of CFD is its ability to provide details on the flow structure, which are commonly very difficult to analyze in experiments. Rao *et al*. (2015) studied the flow and heat transfer characteristics of hemispherical and tear drop

*Corresponding author
Email address: wmakatar@eng.psu.ac.th

dimples by using CFD. The dimensions of hemispherical dimples were similar to the case of Mahmood *et al*. (2000). The results showed details of heat transfer characteristics on the dimple surface and agreed well with experimental results. In addition, Elyyan and Tafti (2008), Kim and Shin (2008), Xie *et al*. (2015), Yoon, Park, Choi, and Ha (2015) used CFD to predict flow and heat transfer with a dimple array in channel flow.

Although the aforementioned studies have focused on arrays of dimples, there is a need to fundamentally understand the effects of single dimple by eliminating the effects of neighboring dimples: lateral, upstream and downstream dimples. In order to eliminate the effects of neighboring dimple effects, many studies, such as Isaev, Kornev, Leontiev, and Hassel (20 10), Isaev, Schelchkov, Leontiev, Baranov, and Gulcova (2016), Kore, Yadav, and Sane (2015), and Xia, Tang, Shi, and Tao (2014) focused on a single dimple.

In this work, hemispherical dimples on a smooth surface were studied to understand the thermal characteristics and flow structures. The aims of present work were to investigate the flow interaction between dimple and lateral dimple, and the effects of hemispherical dimple-to-dimple spacing on flow structure and heat transfer characteristics, by CFD simulations.

2. Methods

ANSYS (Fluent) software was used to simulate the flow and heat transfer characteristics of the cases. A three dimensional (3D) numerical model was created imitating the geometrical details of a wind tunnel used in prior experimental work by Wae-hayee, Tekasakul, Eiamsa-ard, and Nuntadusit (2014) and Wae-hayee, Tekasakul, Eiamsa-ard, and Nuntadusit (2015). The studies Wae-hayee *et al*. (2014) and Wae-hayee *et al*. (2015) were also used for validation of the present CFD results.

2.1 Model of dimples

The model with a row of dimples formed on the inner surface of a rectangular wind tunnel is shown in Figure 1. Fully developed air flow passes through the test section. The origin of Cartesian coordinate system is located at the centerof the middle dimple. The X-axis is in the direction of flow inside the wind tunnel, Y-axis is along the height, and Z-axis is perpendicular to the flow.

The details of a dimple are shown in Figure 2. The diameter of hemispherical dimple was 40 mm, and printed diameter on the surface was D=26.4 mm. The depth of dimple, from the surface to the dimple bottom, was 0.2D as in Isaev *et al*. (2016), Kim *et al*. (2008), Rao *et al*. (2015). The dimple-to-dimple spacing was set to S=1.125D, 1.25D, 1.5D and 2D. The Reynolds number of air flow inside the wind tunnel, based on the hydraulic diameter of the wind tunnel, was fixed at Re_H=20,000 as in Mahmood *et al*. (2000) and Rao *et al*. (2015).

2.2 Wind tunnel

In this work, a wind tunnel was investigated to be able to validate the CFD results, while the experimental measurements have been done only with a smooth wall. The temperature of heat transfer surface of smooth wall was measured using TLC technique. The details of measurements and wind tunnel were given earlier by Wae-hayee *et al*. (2014) and Wae-hayee *et al*. (2015).

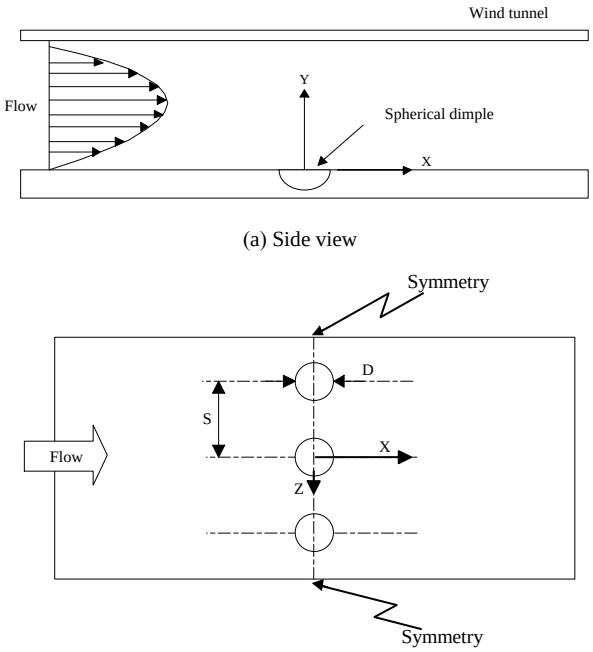

(a) Side view

(b) Top view

Figure 1. The model investigated.

Figure 3 shows the computational model imitating the geometrical details that have been used in the experimental setup of Wae-hayee *et al*. (2014) and Wae-hayee *et al*. (2015). The wind tunnel has a rectangular cross-section consisting of three parts: upstream of the test section (1700 mm), test section (280 mm), and downstream of the test section (490 mm). The length of the upstream section was designed to achieve fully developed flow. The height of model was set at 26.4 mm (1D). The width of wind tunnel was varied depending on the dimple-to-dimple spacing.

The details of simulation grid used in this study are shown in Figure 4. A cut along the centre-line of the dimples is shown to expose the internal grid system. The majority of the mesh had even hexahedral geometries, while uneven hexahedral geometries were used to accommodate the non-uniform surfaces at dimples and their surroundings. Intensive mesh generation was applied at the near wall region to enable accurate prediction

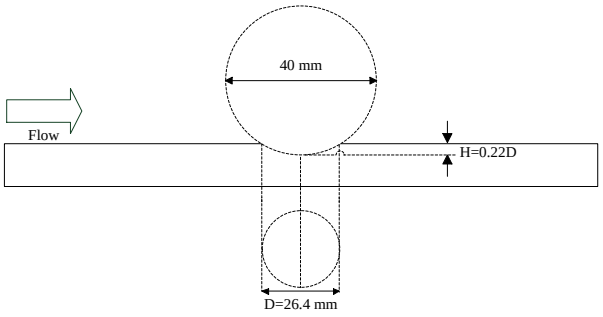

Figure 2. The details of a dimple.

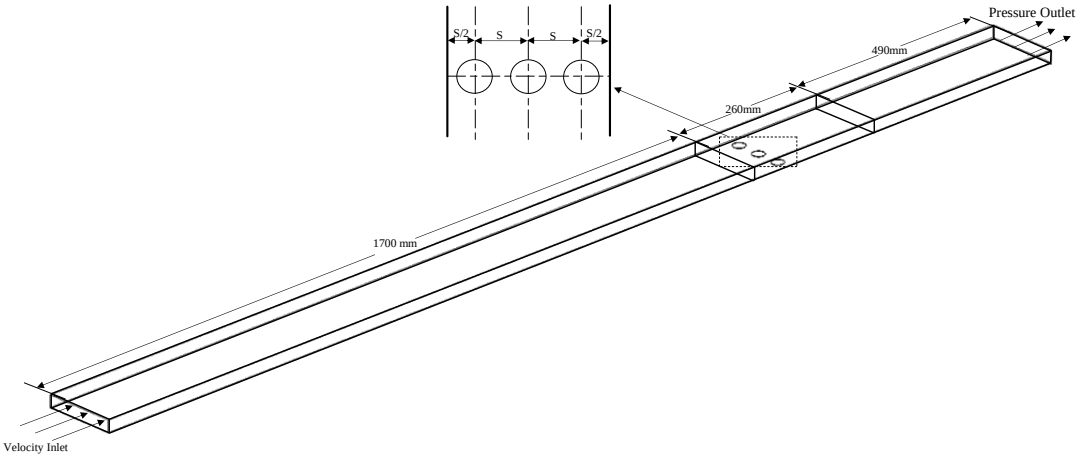

Figure 3. The wind tunnel with spherical dimples.

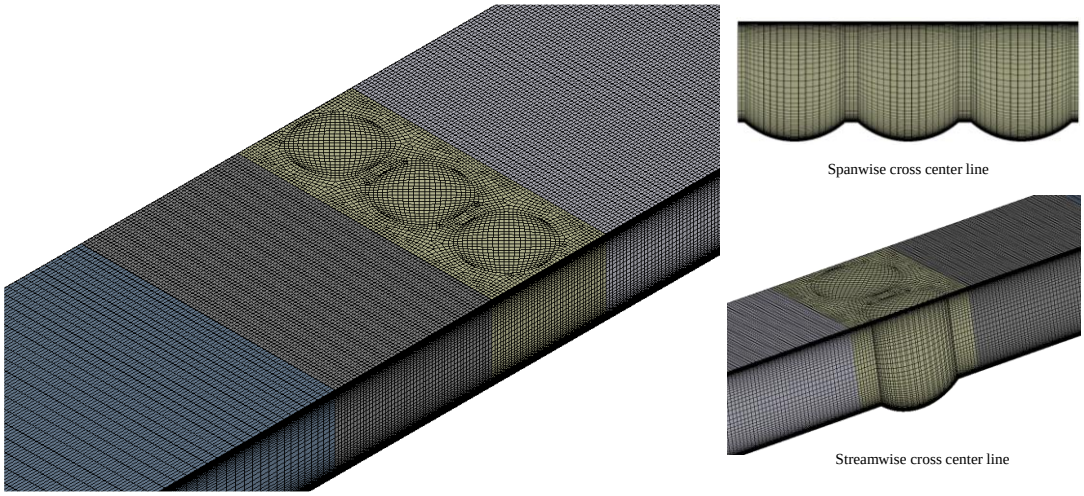

Figure 4. Generated grids.

in the viscous sub layer. In a mesh dependency test, different y+ distributions were considered as shown in Figure 5. The analysis of y+ distribution was considered for the ($-5 \leq X/D \leq 5$) (Z/D=1) and S=2D case. Based on the y+ distributions, 7,294,941 elements were chosen as the computational domain.

2.3 Assumptions and boundary conditions

In the numerical model, the upper and the lower wall had no slip condition imposed. All walls, except for the bottom wall of test section, were insulated for adiabatic conditions. A steady state simulation as in Kore, Yadav, and Sane (2015), Rao, Li, and Feng (2015), Xie, Qu, and Zhang (2015), Xia, Tang, Shi, and Tao (2014), of incompressible flow with constant thermal properties and no gravitational effects was employed in this current study. The inlet was set to have uniform velocity with Re_H=20,000 and the air was at 25 ^oC. The pressure at outlet was set at 1 atm. Both of the lateral walls were set as symmetry. The heat transfer surface with dimples was set at a constant heat flux ($\dot{q}$ =150 W/m^2).

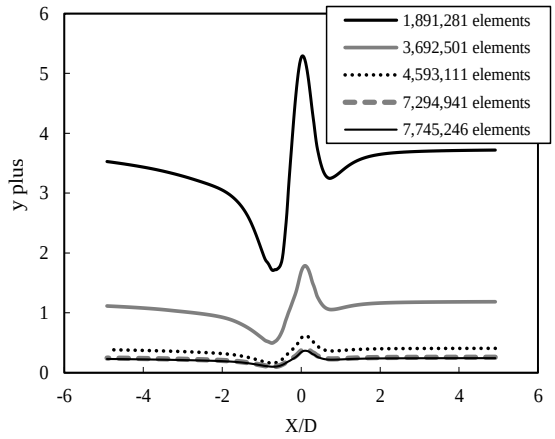

Figure 5. y plus distributions on the surface over the dimple interval interval($-5 \leq X/D \leq 5$) (Z/D=1) with S=2D.

2.4 Numerical calculation method

A 3-D numerical model based on the finite volume method was adopted to solve the governing equations with boundary conditions. The details can be found in Versteeg and Malalasekera (2007). Fluid flow and heat transfer were solved using a Shear Stress Transport (SST) k-ω turbulence model because it tends to be accurate with moderate computational cost, Versteeg *et al*. (2007). The suitability of this turbulence model has also been reported in various studies, such as Rao *et al*. (2015), Wae-hayee *et al*. (2015), Xie *et al*. (2015).

The solution used Semi Implicit Method for Pressure-Linked Equations (SIMPLE) algorithm with second order upwind for all spatial discretizations. As convergence criteria, the root mean square (RMS) residuals of continuity and energy equations were required to be better than 10^{-8} and that of momentum equation was required to reach 10^{-5}, Rao *et al*. (2015) and Wae-hayee *et al*. (2015).

2.5 Nusselt number calculation

The heat transfer coefficient, h, could be calculated from:

$$h = \frac{\dot{q}}{T_{wall} - T_{air}} \quad (1)$$

where, $\dot{q}$ is heat flux, T_{wall} is wall temperature and T_{air} is air temperature.

The Nusselt number, Nu, is calculated from:

$$Nu = \frac{hD_H}{k} \quad (2)$$

where D_H is the hydraulic diameter of the tunnel and k is the thermal conductivity of the air.

3. Results and Discussion

3.1 Verification of simulation

For verification, the well-known Dittus-Boelter correlation, $Nu_o = 0.23\mathrm{Re}^{0.8}\,\mathrm{Pr}^{0.4}$ where Re and Pr are Reynolds number and Prandtl number, was used to compare internal heat transfer in the smooth channel, Rao, Li, and Feng (2015). The average Nusselt number versus Reynold number for smooth wind tunnel were compared between the correlation, the experimental results, and the CFD results in this work, as shown in Figure 6. The current data agrees well with the correlation and with the experimental results, and overall heat transfer increases with the Reynolds number. Discrepancies were found in the same range as in the work of Rao *et al*. (2015).

The velocity profiles of air flow in wind tunnel by height before entering the test section at Z/D=0 are shown in Figure 7. The velocity profiles over smooth surfaces were analyzed both experimentally and by simulation. In the wind tunnel experiment, a Pitot tube was fixed at Z/D=0 and X/D =2.84 and the air velocities were identical to those from numerical analysis. The experimental results were also used to verify the CFD results with the setup in earlier work by Wae-hayee (2014) and Wae-hayee *et al*. (2015). Good agreement of the velocity profiles between CFD and experiment can be observed. The highest velocity is at the centre of the wind tunnel. The blunt velocity profiles are typical of turbulent flow.

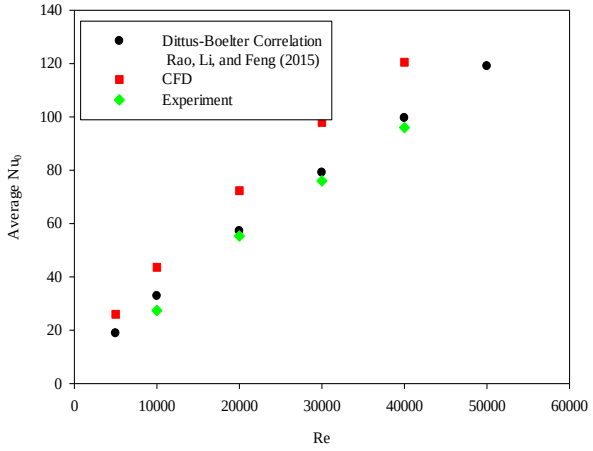

Figure 6. Average Nusselt number versus Reynold number from prior experiments and from current CFD simulations.

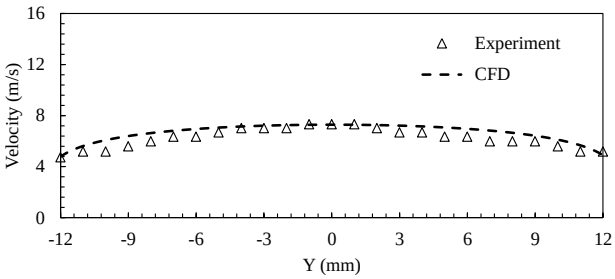

Figure 7. The velocity profiles of flow before entering the test section (Z/D=0 and 1,560 mm from the inlet).

3.2 Flow characteristics

Streamlines of flow over a dimpled surface are shown in Figure 8. The figure clearly indicates the circulation flow in the dimple cavities. The figure also shows that the circulation was occurring at the upstream portion of the dimple cavity. This can be further confirmed in Figure 9, which shows a streamline inside the dimple cavity. The static circulation flow acts as a thermal insulator reducing heat transfer in upstream portion of the dimpled surface, as will be further discussed later.

In Figure 8, the upstream streamline (before passing a dimple) is straight whereas downstream streamlines (immediately after passing dimple, X/D ≈ 0.5) separated from the centre-line and tended to the lateral side. This was an effect of the longitudinal vortex pair in flow after passing the dimple, as reported earlier by Ligrani *et al*. (2003), Mahmood *et al*. (2000), Mahmood and Ligrani (2002). Here, it can be noted that for the case of S=1.125D shown in Figure 8 (a), the flow tendency to the lateral sides of this vortex pair seems to be lesser than in other cases, due to confinement by neighboring vortex pair with close dimple-to-dimple spacing.

Streamline passing the centre of middle dimple (Z/D =0) for the case of S=1.125D is shown in Figure 9. The figure

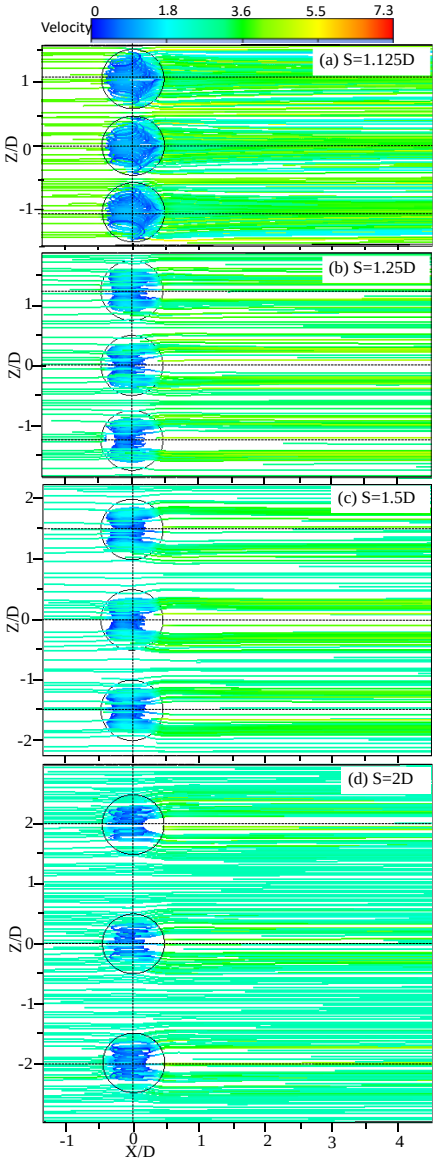

Figure 8. Streamlines above the surface of dimples.

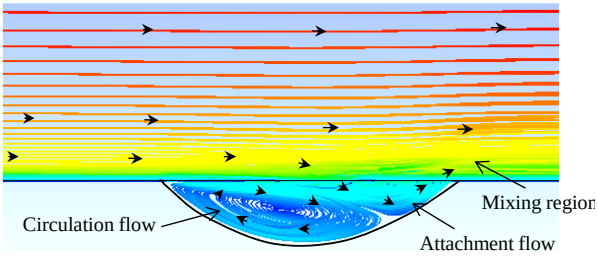

Figure 9. Streamlines at the center plane of middle dimple (S/D= 1.125).

shows the flow inside the dimple. It can be observed that stationary circulation occurred upstream of the dimple, while attachment occurred downstream of it. The attachment increases heat transfer as will be further discussed in the next section.

Velocity vectors in the Y-Z plane are shown in Figure 10. At X/D=0.5 (immediately downstream of dimple) for all S/D cases (Figure 10 (a), (e), (i) and (m)), the vectors rose upward from bottom of dimple to the upper surface of wind tunnel in dimple area. Then, at X/D=1.0, these frames show the different characteristics of velocity vectors for every S/D due to the main flow: (1) S=1.125D (Figure 10(b)), a longitudinal vortex pair can be detected clearly; (2) S=1.25D (Figure 10(f)), a longitudinal vortex pair was depressed by the main flow and cannot be detected clearly; (3) S=1.5D (Figure 10(j)), velocity vectors attached laterally on the smooth downstream surface; (4) S=2D (Figure 10(n)), the attachment velocity turned upward from the bottom surface. All this can be seen from the white bold arrow sketches in the figures.

In the case S=1.125D, the longitudinal vortex pair was confined by neighboring ones due to short dimple-to-dimple spacing, whereas with S≥1.25D a longitudinal vortex pair was separated by attachment flow. Sketches of the flow structures downstream of dimples,with short and large dimple-to-dimple spacings,are shown in Figure 11. A sketch of flow structure for the case of a dimple array was presented by Mahmood *et al*. (2000). The longitudinal vortex pair downstream was similar as in this study, as shown in Figure 11(a), in the case of short dimple-to-dimple spacing. When dimple-to-dimple spacing is larger, the vortex-to-vortex spacing is also larger replacing the attachment flow at the middle between them, as shown in Figure 11(b).

3.3 Heat transfer

Contours of Nusselt numbers on the surface are shown in Figure 12. In the dimples, it is found that Nusselt numbers were high on the downstream portion of a dimple, especially near the rear rim of the dimple, because of the attachment flow shown previously in Figure 9. On the other hand, Nusselt numbers were low on the upstream portion of a dimple due to stationary circulation. Attachment and circulation flows increase or decrease the Nusselt number on a dimple surface as previously discussed by Rao *et al*. (2015) and Xie *et al*. (2015). For the case of S≥1.25D (Figure 12 (b)-(d)), the Nusselt numbers on smooth surface downstream of the dimples were high in a single region, whereas in the case S=1.125D (Figure 12 (a)) high values come up in two regions. The double peak regions are generated by the longitudinal vortex pair that was confined, with strong circulation above the heat transfer surface and effective removal of heat from the surface.

Nusselt number distributions in the spanwise direction (Z/D) are shown in Figure 13. Generally, in every S/D case, the Nusselt number peaked at just downstream of the dimples and then decreased downstream. At X/D=0.5, the peaks of Nusselt number for S≥1.25D were extremely high, but the peak areas were very small. In contrast, with S=1.125D the peaks seem blunt and with larger areas. This was the initiation of a single peak region (for S≥1.25D) by attachment flow, and blunt double peaks (for S=1.125D) from the effect of closing vortex pair spacing. In addition, for S≥1.25D the secondary peak can be detected, especially for the case of S=2D (Figure 13(d)). This can be attributed to the longitudinal vortex pair that was separated by attachment flow. With S≥1.25D the attachment flow was dominant over the longitudinal vortex pair giving a single peak that is more obvious than the secondary peak.

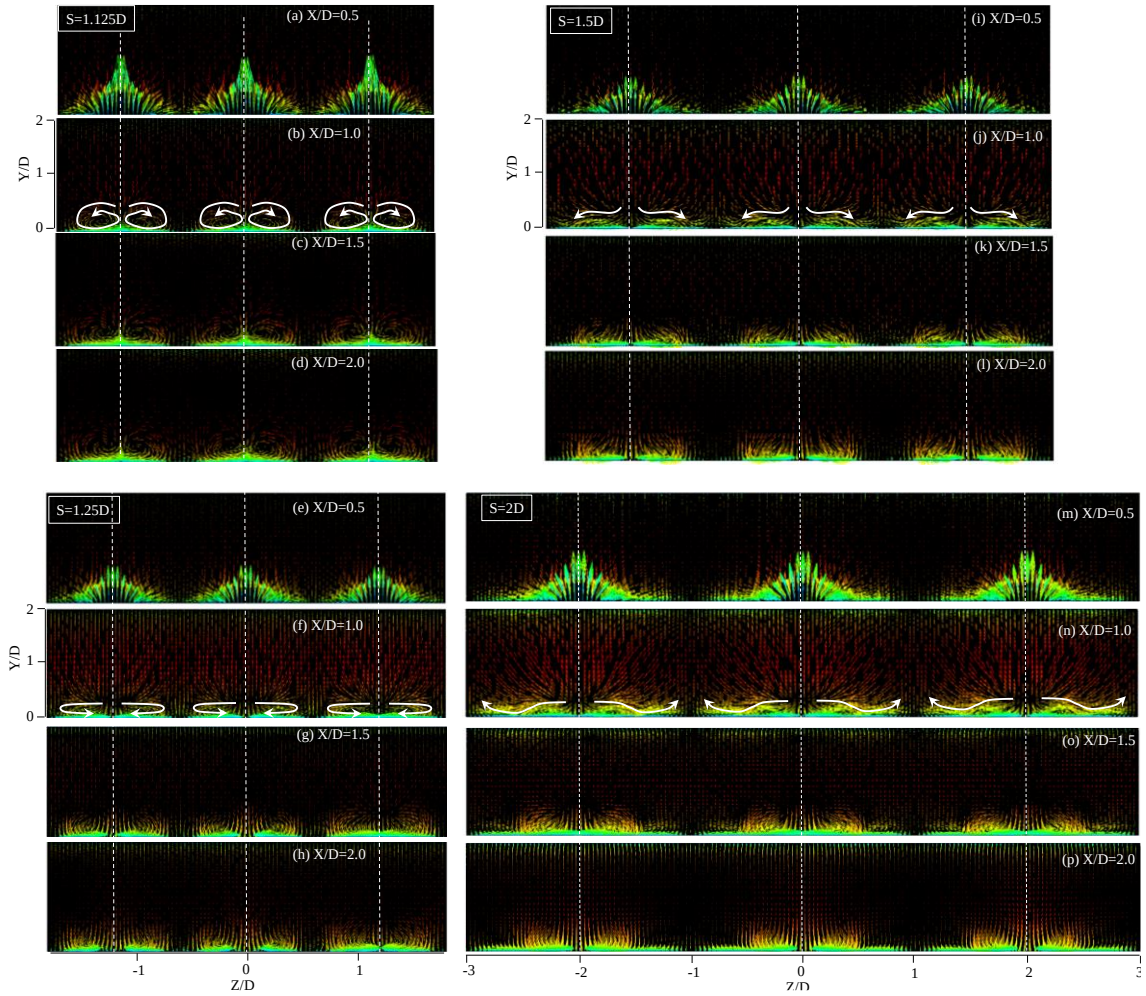

Figure 10. Velocity vectors in the Y-Z plane (Dashed straight line is the center of the dimples).

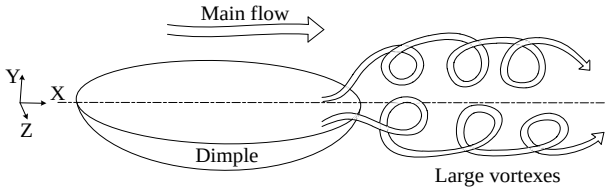

(a) Short dimple-to-dimple spacing

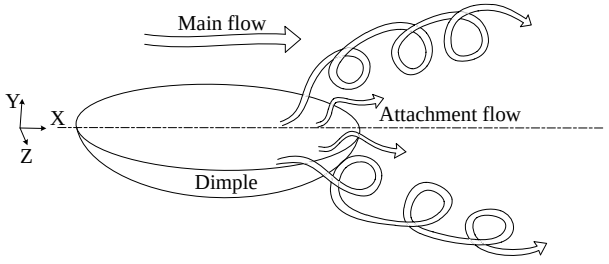

(b) Large dimple-to-dimple spacing

Figure 11. Sketches of flow structures downstream from a dimple.

4. Conclusions

In this study, the dimple-to-dimple spacing (1.125D ≤S≤2D)effects on flow structure and heat transfer in an internal flow were investigated. The results show that at S=1.125 D, a longitudinal vortex pair extending downstream from the dimples was confined by neighboring vortex pairs. In this case, the area with high Nusselt number had two peaks per dimple, due to the vortex pair. For S≥1.25D, the longitudinal vortex pair was separated by an attachment flow between them, so that there was a single Nusselt number peak per dimple. In addition, with S≥1.25D the longitudinal vortex pair still affected the Nusselt number giving secondary peaks, especially with the largest dimple-to-dimple spacing, S=2D.

Nomenclature

D_H : Hydraulic diameter (m)
h : Convective heat transfer coefficient (W/m^2.K)
T_w : Wall temperature (^{o}C)
T_{air} : Inlet air temperature (^{o}C)
$\dot{q}$: Heat flux (W/m^2)

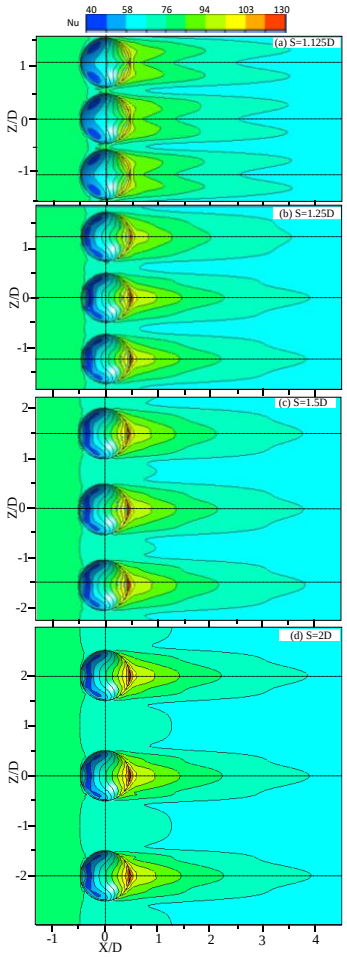

Figure 12. Nusselt number distributions on the surface (Re_H=20,000).

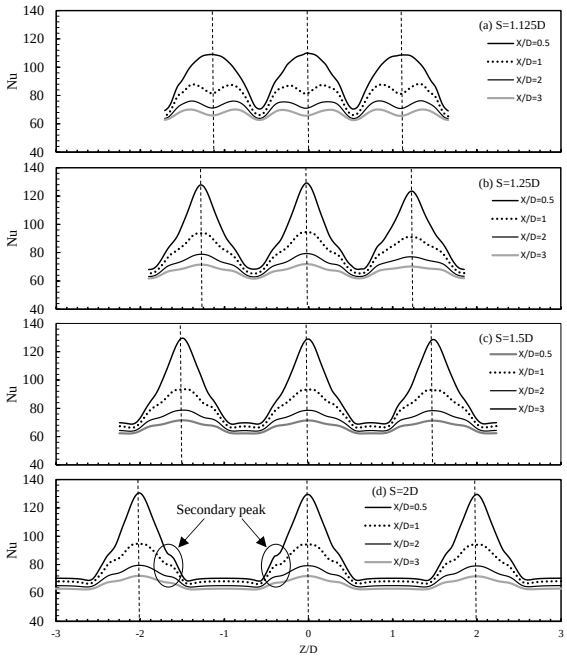

Figure 13. Nusselt number distributions in spanwise direction, Z/D (Dashed straight line is the center of the dimples).

Acknowledgements

The research grant was supported by the Research and Development Office (RDO), Prince of Songkla University, grant No. ENG590725S.

References

Elyyan, M. A., & Tafti, D. K. (2008). Large eddy simulation investigation of flow and heat transfer in a channel with dimples and protrusions. *Journal of Turbomachinery*, *130*, 041016-1-9. doi:10.1115/1.2812412

Heo, S. C., Seo, Y. H., & Kang, B. S. (2011). Formability evaluation of dimple forming process based on numerical and experimental approach. *Journal of Mechanical Science and Technology*, *25*(2), 429-439. Retrieved from https://link.springer.com/article/10.1007/s12206-010-1233-3

Isaev, S. A., Kornev, N. V., Leontiev, A. I., & Hassel, E. (2010). Influence of the Reynolds number and the spherical dimple depth on turbulent heat transfer and hydraulic loss in a narrow channel. *International Journal of Heat and Mass Transfer*, *53*(1–3), 178-197. doi:10.1016/j.ijheatmasstransfer.2009.09.042

Isaev, S. A., Schelchkov, A. V., Leontiev, A. I., Baranov, P. A., & Gulcova, M. E. (2016). Numerical simulation of the turbulent air flow in the narrow channel with a heated wall and a spherical dimple placed on it for vortex heat transfer enhancement depending on the dimple depth. *International Journal of Heat and Mass Transfer*, *94*, 426-448. doi:10.1016/j.ijheatmasstransfer.2015.11.002

Kim, K. Y., & Shin, D. Y. (2008). Optimization of a staggered dimpled surface in a cooling channel using Kriging model. *International Journal of Thermal Science*, *47*(11), 1464-1472. doi:10.1016/j.ijthermalsci.2007.12.011

Kore, S. S., Yadav, R. J., & Sane, N. K. (2015). Investigations of effect of dimple depth on heat transfer and fluid flow within rectangular channel. *Procedia Engineering*, *127*, 1110-1117. doi:10.1016/j.proeng.2015.11.473

Kurniawan, R., Kiswanto, G., & Ko, T. J. (2017). Surface roughness of two-frequency elliptical vibration texturing (TFEVT) method for micro-dimple pattern process. *International Journal of Machine Tools and Manufacture*, *116*, 77-95. doi:10.1016/j.ijmachtools.2016.12.011

Lan, J., Xie, Y., & Zhang, D. (2011). Effect of leading edge boundary layer thickness on dimple flow structure and separation control. *Journal of Mechanical Science and Technology*, *25*(1), 3243-3251. doi:10.1007/s12206-011-0823-z

Ligrani, P. M., Harrison, J. L., Mahmmod, G. I., & Hill, M. L. (2001). Flow structure due to dimple depressions on a channel surface. *Physics of Fluids*, *13*(11), 3442-3451. doi:10.1063/1.1404139

Ligrani, P. M., Oliveira, M. M., & Blaskovich, T. (2003). Comparison of heat transfer augmentation techniques, *AIAA Journal*, *41*(3), 337-362. doi:10.2514/2.1964

Mahmood, G. I., Hill, M. L., Nelson, D. L., Ligrani, P. M., Moon, H. K., & Glezer, B. (2000). Local heat transfer and flow structure on and above a dimpled surface in a channel. *Journal of Turbomachinery*, *123*(1), 115-123.

doi:10.1115/1.1333694

Mahmood, G. I., & Ligrani, P. M. (2002). Heat transfer in a dimpled channel: combined influences of aspect ratio, temperature ratio, Reynolds number, and flow structure. *International Journal of Heat and Mass Transfer*, *45*(10), 2011-2020. doi:10.1016/S0017-9310(01)00314-3

Rao, Y., Li, B., & Feng, Y. (2015). Heat transfer of turbulent flow over surfaces with spherical dimples and teardrop dimples. *Experimental Thermal and Fluid Science*, *61*, 201-209. doi:10.1016/j.expthermflusci.2014.10.030

Shin, S., Lee, K. S., Park, S. D., & Kwak, J. S. (2009). Measurement of the heat transfer coefficient in the dimpled channel: effects of dimple arrangement and channel height. *Journal of Mechanical Science and Technology*, *23*(3), 624-630. doi:10.1007/s12206-008-1211-1

Versteeg, H. K., & Malalasekera, W. (2007). *An Introduction to Computational Fluid Dynamics, Second Edition*. Essex, England: Pearson Prentice Hall.

Vorayos, N., Katkhaw, N., Kiatsiriroat, T., & Nuntaphan, A. (2016). Heat transfer behavior of flat plate having spherical dimpled surfaces. *Case Studies in Thermal Engineering*, *8*, 370-377. doi:10.1016/j.csite.2016.09.004

Wae-hayee, M., Tekasakul, P., Eiamsa-ard, S., & Nuntadusit, C. (2014). Effect of cross-flow velocity on flow and heat transfer characteristics of impinging jet with low jet-to-plate distance. *Journal of Mechanical Science and Technology*, *28*(7), 2909-2917. doi:10.1007/s12206-014-0534-3

Wae-hayee, M., Tekasakul, P., Eiamsa-ard, S., & Nuntadusit, C. (2015). Flow and heat transfer characteristics of in-line impinging jets with cross-flow at short jet-to-plate distance. *Experimental Heat Transfer*, *28*, 511-530. doi:10.1080/08916152.2014.913091

Won, S. Y., & Ligrani, P. M. (2007). Flow characteristics along and above dimpled surfaces with three different dimple depths within a channel. *Journal of Mechanical Science and Technology*, *21*, 1901-1909. doi:10.1007/BF03177447

Won, S. Y., Zhang, Q., & Ligrani, P. M. (2005). Comparisons of flow structure above dimpled surfaces with different dimple depths in a channel. *Physics of Fluids*, *17*(4), 045105-1-9. doi:10.1063/1.1872073

Xia, H. H., Tang, G. H., Shi, Y., & Tao, W. Q. (2014). Simulation of heat transfer enhancement by longitudinal vortex generators in dimple heat exchangers. *Energy*, *74*, 27-36. doi:10.1016/j.energy.2014.02.075

Xie, Y., Qu, H., & Zhang, D. (2015). Numerical investigation of flow and heat transfer in rectangular channel with teardrop dimple/protrusion. *International Journal of Heat and Mass Transfer*, *84*, 486-496. doi:10.1016/j.ijheatmasstransfer.2015.01.055

Yoon, H. S., Park, S. H., Choi, C., & Ha, M. Y. (2015). Numerical study on characteristics of flow and heat transfer in a cooling passage with a tear-drop dimple surface. *International Journal of Thermal Science*, *89*, 121-135. doi:10.1016/j.ijthermalsci.2014.11.002